# Experimental and Theoretical Studies on the Complex Formed between $H_2S$ and $O_2^-$

**Andrew J. Bell*,† and Timothy G. Wright*,‡**

*Dstl, Porton Down, Salisbury, Wiltshire, United Kingdom, SP4 0JQ and School of Chemistry, University of Nottingham, University Park, Nottingham, United Kingdom, NG7 2RD*

*Received: September 9, 2004*

The negative cluster ion with $m/z = 66$, produced when $H_2S$ gas was introduced into an ion mobility spectrometer at atmospheric pressure, has been investigated using both collision-induced dissociation as well as ab initio and density functional calculations. The results from both studies indicate that the identity of the ion is consistent with the clustering of the superoxide anion, $O_2^-$, and $H_2S$, and that the structure of the negative ion is more accurately represented as "$HS-HO_2$", that is, proton transfer has occurred from $H_2S$ to the superoxide anion. The evidence is that this proton transfer has a small or negligible barrier. We calculate a binding energy, $D_e$, for the $HS-HO_2$ complex of 14.4 kcal mol$^{-1}$.

## I. Introduction

Hydrogen sulfide, $H_2S$, is produced in the human body and has several roles, including an effect on memory.[1,2] Patients with Alzheimer's disease exhibit decreased levels of $H_2S$ in the brain,[3] whereas Down syndrome sufferers have increased levels of $H_2S$ metabolites.[4] Recent studies[5] in vitro have demonstrated that $H_2S$ directly scavenges free radicals of oxygen, such as $O_2^-$. It is of interest, therefore, to study the interaction between an isolated $H_2S$ molecule and an $O_2^-$ anion to understand the fundamental interactions that are occurring.

Ion mobility spectrometry (IMS) is a useful tool for the detection of trace species, including pollutants arising from industry,[6] chemical warfare agents,[7] and explosives.[8] Although the implementation of the technique in handheld instruments is relatively straightforward, the detailed understanding of the origin of a signal relies on an understanding of the ion−molecule chemistry occurring, as well as the transport of the ions through the bath gas (in most applications, often air containing significant concentrations of water vapor). The chemistry involved covers both positive and negative modes, and here we concentrate on the latter.

In the negative mode of an ion mobility spectrometer, cluster formation of the analyte with $O_2^-$ is one of the main mechanisms for forming product ions. In water-based IMS (i.e., an IMS system with air used as the carrier and drift gases, with no other "dopant" added), the $H_2O-O_2^-$ ion is formed (along with larger hydrates of $O_2^-$, together forming part of the reactant ion peak or RIP). This is one of the few ions for which detailed structural information is known. In the present work, we concentrate on the cluster ion that appears in negative mode when $H_2S$ is introduced into an atmospheric pressure ion mobility spectrometer and show that this occurs from the interaction between $O_2^-$ and $H_2S$. We describe both the experiments and a series of theoretical calculations aimed at elucidating the structure of the ion observed.

* To whom correspondence should be addressed. E-mail: Timothy.Wright@nottingham.ac.uk (T.G.W.); ATBELL@dstl.gov.uk (A.J.B.); fax: +44 115 951 3555.

† Dstl.

‡ University of Nottingham.

## II. Experimental Details

The IMS/MS instrument (PCP, FL) used in the initial experiments was maintained at a temperature of 35 °C and at atmospheric pressure (748 Torr), with a water vapor concentration of ca. 100 ppm (measured using a Si-grometer, MCM, Wetherby, U.K.). The atmospheric pressure drift tube is coupled, via a 25 $\mu$m diameter orifice, to a chamber housing a quadrupole mass spectrometer. The mass spectrometer was tuned for external ion analysis. The ionization source used was a $^{63}$Ni 10 mCi $\beta$-emitter. Concentrations of $H_2S$ (99.5% pure, Aldrich, U.K.) studied were between ca. 0.01 ppm and 1 ppm. The $H_2S$ was introduced into the carrier gas flow by use of a syringe and syringe drive. The mass spectrometer was used in three configurations: (1) with the IMS cell shutter grid open, the mass spectrometer was scanned (between $m/z$ values of 30 and 180) to determine the intensity and $m/z$ values of all ions contributing to the IMS spectrum; (2) with the IMS cell operating normally, the mass spectrometer was set to allow all $m/z$ values to traverse the analyzer, resulting in a conventional ion mobility spectrometer with the mass spectrometer simply acting as the ion detector; (3) with the IMS cell operating normally, the mass spectrometer was tuned to a specific $m/z$ value determined from the initial mass scan, hence enabling the generation of a mobility spectrum for a specific ion (thus determining the position of that ion species in the mobility spectrum).

To characterize further the ion species formed, a second IMS/MS system was used. It was built such that a variable potential could be set up at the interface between the home-built IMS cell and the mass spectrometer (SXP Elite, VG Quadrupoles, U.K.). The orifice (60 $\mu$m diameter) could be biased with respect to a plate placed in front of the cone that forms the entrance to the ion optics of the quadrupole rods of the mass spectrometer. It is well known that the application of potentials at supersonic expansions involving ionic species can cause fragmentation of cluster ions (so-called "cluster-busting").[9] In these experiments, the ionization source was a corona discharge source (corona current ca. 10 $\mu$A). The ionization source was set up in a reverse flow mode to reduce the effect of ozone produced at the corona tip,[10] thus allowing the system to mimic the chemistry observed when using a radioactive ionization source; the negative ions produced in corona discharges under dry and "wet" conditions

10.1021/jp045930+ CCC: $27.50 
Published on Web 10/28/2004

has recently been investigated.[11] The water vapor concentration in these experiments was approximately 15 ppm, and the temperature was approximately 300 K.

$H_2S$ was added to the carrier flow of the IMS cell to give a concentration of 10 ppm at the ionization source. The IMS cell was run with its shutter grid open throughout the experiments, thus enabling all ions to be detected. The mass spectrometer was scanned from 30 to 100 *m*/*z*.

### III. Calculational Details

Initial optimizations were carried out in $C_{2v}$ symmetry, with H-bonds between the two H atoms of $H_2S$ and the oxygens of $O_2^-$ (this may be viewed as a bifurcated H-bond, if the $O_2^-$ moiety is considered as the bonding species). These optimizations employed the 6-311++G** basis set, and the MP2, B3LYP, MP4(SDQ), and QCISD methods were employed; second derivatives allowed harmonic vibrational frequencies to be obtained. Further optimizations were then performed employing the aug-cc-pVTZ basis set and employing the UMP2, B3LYP, and QCISD methods; for the first two cases, harmonic vibrational frequencies were also calculated.

Preliminary calculations then moved onto considering $C_s$ structures in line with expectations based on the complex formed between $H_2O$ and $O_2^-$ (refs 12 and 13); however, these $C_s$ structures gave rise to one imaginary vibrational frequency, suggesting that the energy minimum was nonplanar. Consequently, $C_1$ structures were employed, and further details will be provided below.

Finally, binding energies of the complex were calculated at the RCCSD(T)/aug-cc-pVTZ level of theory; these calculations will also be described in more detail below.

Optimizations and harmonic vibrational frequencies were carried out employing the Gaussian03 package.[14] Unrestricted electronic wave functions were employed, with $\langle S^2 \rangle$ values of $<0.78$ being obtained, indicating that spin contamination was negligible. The RCCSD(T) calculations were carried out with MOLPRO.[15] In all calculations, the frozen-core approximation was employed.

### IV. Results

**Experiments.** In the initial ion mobility experiments (see Figure 1), at the lowest concentration of $H_2S$ (0.01 ppm) the major product ion had a reduced mobility ($K_0$) of 2.48 $cm^2\ V^{-1}\ s^{-1}$ and *m*/*z* value of 66. This ion was considered to have the empirical structure $H_2SO_2^-$. At the higher concentrations (0.3 and 1.0 ppm), a peak at a mobility of 2.47 $cm^2\ V^{-1}\ s^{-1}$, also assigned to $H_2SO_2^-$, was observed. In addition, a small contribution to the mobility spectrum from an ion with $K_0 =$ 2.95 $cm^2\ V^{-1}\ s^{-1}$ and an *m*/*z* value of 33 was also observed. This was tentatively assigned to $SH^-$.

In the second set of experiments, at low potentials between the orifice and plate (3 V) an ion with an *m*/*z* value of 66 (again assigned to a species with empirical formula, $H_2SO_2^-$) was the dominant peak in the mass spectrum. At a higher potential difference of 10 V, the intensity of the ion at *m*/*z* value 66 reduced significantly with a concomitant rise in the intensity of an ion at an *m*/*z* value of 33 ($HS^-$), see Figure 2. There is a small peak at $m/z = 35$ and another at $m/z = 68$ which are attributable to the $^{34}S$ isotopomers for each of the main ions, and the presence of these features and their relative intensity to the main isotopomer peak confirm the species as containing a single sulfur atom. From these results, we deduce that the observed ion with $m/z = 66$ is actually $HS{-}HO_2$ and that consequently a proton has been transferred from $H_2S$ to $O_2^-$.

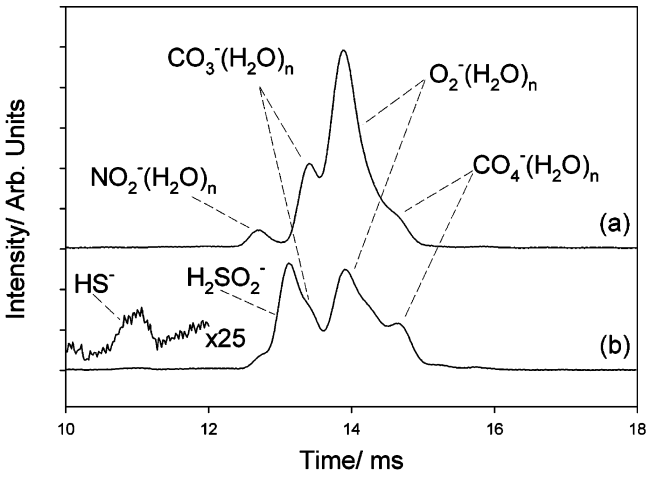


**Figure 1.** Ion mobility spectra for (a) the negative reactant ion peak (RIP) in air, standard ions are indicated, and (b) 0.01 ppm $H_2S$ in air, negative mode. The additional ions produced from the introduction of the $H_2S$ are indicated in b. The identification of the ions and the correlation to the ion mobility peaks were determined from mass spectrometry and tuned ion mobility measurements, respectively. Mobility peaks correspond to ions with several levels of hydration. The $K_0$ values are ($cm^2\ V^{-1}\ s^{-1}$) (a) $CO_4^-(H_2O)_n$, 2.21; $O_2^-(H_2O)_n$, 2.47; $CO_3^-(H_2O)_n$, 2.43; $NO_2^-(H_2O)_n$, 2.55; (b) "$H_2SO_2$", 2.47; $HS^-$, 2.95.

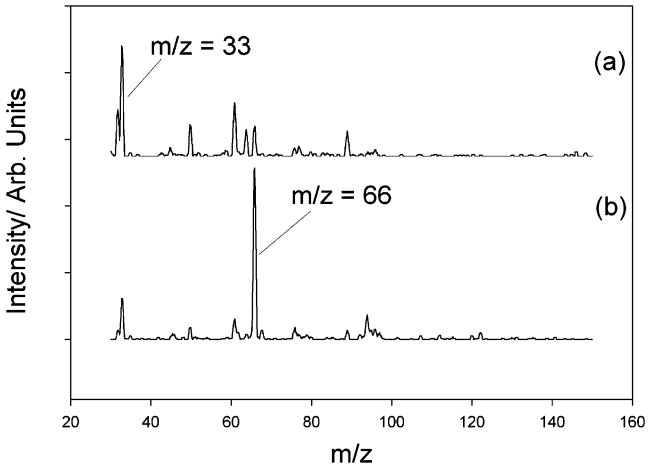


**Figure 2.** Negative mode mass spectra obtained from the ions produced by a corona discharge source in air in the presence of $H_2S$. The voltage drop between the orifice and the mass spectrometer plate were (a) 10 V and (b) 3 V. The increased potential difference in a leads to a rise in fragmentation of the $m/z = 66$ ion to produce a concomitant rise in the $m/z = 33$ signal. (The peak immediately to the right of the $m/z =$ 33 peak corresponds to $H^{34}S^-$; similarly, the peak to the right of the $m/z = 66$ peak corresponds to "$H_2{}^{34}S{-}O_2^-$".)

Collisions between $I^-$ and $H_2S$[16] produce $HS^-$ once the reaction endothermicity has been overcome. We consider the reaction exothermicity for the proton transfer below.

**Optimized Geometries and Harmonic Vibrational Frequencies.** Table 1 shows the optimized geometries and harmonic vibrational frequencies obtained when a $C_{2v}$ constraint was imposed upon the geometry. Although the MP2 calculations indicated that a minimum energy geometry has been obtained, using both the 6-311++G** and aug-cc-pVTZ basis sets, the MP4(SDQ), B3LYP, and QCISD methods indicate that the $C_{2v}$ structure is actually a saddle point. (Interestingly, similar behavior was observed in our recent calculations on $O_2^-{\cdot}H_2O$,[13] where the MP2 method indicated a $C_{2v}$ minimum, whereas other levels of theory led to a $C_s$ minimum.) The imaginary frequency represents a distortion in-plane, and consequently we performed

**TABLE 1: Optimized Geometry of $C_{2v}$-Constrained $O_2^- - H_2S$**

| | 6-311++ G** | | | | aug-cc-pVTZ | | |
|---|---|---|---|---|---|---|---|
| parameter | UMP2 | UMP4(S DQ) | QCISD | B3LYP | UMP2 | QCISD | B3LYP |
| $R_{SH}$/Å | 1.362 | 1.355 | 1.356 | 1.388 | 1.386 | 1.365 | 1.386 |
| $R_{OH}$/Å | 1.942 | 2.041 | 2.052 | 1.922 | 1.802 | 1.977 | 1.907 |
| $R_{OO}$/Å | 1.346 | 1.335 | 1.332 | 1.325 | 1.344 | 1.330 | 1.324 |
| $\angle_{HSH}$/° | 81.0 | 83.7 | 83.9 | 80.1 | 76.5 | 82.4 | 79.8 |
| $\angle_{SHO}$/° | 133.3 | 131.5 | 131.3 | 133.0 | 135.8 | 132.0 | 133.3 |
| energy/$E_h$ | −548.903 380 | −548.926 299 | −548.92 8007 | −549.845669 | −549.071459 | −549.093288 | −549.865386 |
| $\omega_1$ ($a_1$) | 2565 | 2621 | 2610 | 2385 | 2389 | | 2380 |
| $\omega_2$ ($a_1$) | 1098 | 1168 | 1186 | 1196 | 1104 | | 1194 |
| $\omega_3$ ($a_1$) | 1024 | 1086 | 1095 | 1071 | 941 | | 1045 |
| $\omega_4$ ($a_1$) | 189 | 179 | 178 | 224 | 230 | | 2207 |
| $\omega_5$ ($a_2$) | 341 | 287 | 280 | 404 | 452 | | 403 |
| $\omega_6$ ($b_1$) | 580 | 535 | 532 | 609 | 658 | | 606 |
| $\omega_7$ ($b_2$) | 2650 | 2579 | 2541 | 2210 | 2538 | | 2197 |
| $\omega_8$ ($b_2$) | 561 | 282 | 279 | 432 | 776 | | 422 |
| $\omega_9$ ($b_2$) | 302 | 226*i* | 324*i* | 268*i* | 362 | | 315*i* |

**TABLE 2: Optimized Geometry of Unconstrained "$O_2^- - H_2S$"**

| | 6-311++G** | | | aug-cc-pVTZ | |
|---|---|---|---|---|---|
| | MP2 | QCISD | B3LYP | MP2 | B3LYP |
| $R_{SH1}$ | 1.339 | 1.343 | 1.351 | 1.339 | 1.347 |
| $R_{SH\ 2}$ | 1.894 | 1.962 | 1.936 | 1.894 | 1.947 |
| $R_{O1H2}$ | 1.064 | 1.034 | 1.064 | 1.064 | 1.060 |
| $R_{O1O2}$ | 1.299 | 1.331 | 1.325 | 1.299 | 1.325 |
| $\theta_{H2SH1}$ | 91.8 | 94.2 | 94.0 | 91.8 | 93.8 |
| $\theta_{SH2O1}$ | 175.3 | 174.5 | 174.6 | 175.3 | 173.4 |
| $\theta_{H2O1O2}$ | 107.3 | 106.8 | 108.3 | 107.3 | 108.0 |
| $d_{H1SH2O1}$ | −179.6 | −161.0 | −179.9 | −179.6 | −179.8 |
| $d_{SH2O1O2}$ | 179.5 | 179.2 | 176.6 | 179.5 | 179.9 |
| energy | −548.91342 8 | −548.94698 4 | −549.86114 4 | −549.082389 | −549.882532 |
| $\omega_1$ | 2775 | | 2641 | 2747 | 2654 |
| $\omega_2$ | 2115 | | 2170 | 2134 | 2207 |
| $\omega_3$ | 1576 | | 1536 | 1552 | 1523 |
| $\omega_4$ | 1395 | | 1199 | 1388 | 1201 |
| $\omega_5$ | 802 | | 788 | 822 | 764 |
| $\omega_6$ | 394 | | 381 | 384 | 376 |
| $\omega_7$ | 292 | | 274 | 288 | 269 |
| $\omega_8$ | 140 | | 138 | 137 | 139 |
| $\omega_9$ | 25 | | 102 | 63 | 92 |

some preliminary calculations with $C_s$ symmetry. These calculations converged to a $C_s$ stationary point, but this time (and somewhat surprisingly) the imaginary vibrational frequency was out-of-plane; in addition, it was clear from the charge and spin populations that the system was no longer an $O_2^-$ moiety interacting with $H_2S$ but actually $HS^-$ interacting with $HO_2$.

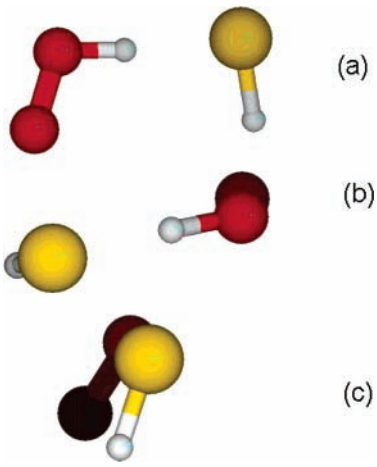


**Figure 3.** Three views of the $C_1$ optimized geometry showing the near planarity of the $HO_2-S$ and that the $HS^-$ is twisted away from this plane: (a) from above; (b) from the side; (c) end on. The labeling of the atoms is used in Table 2, to identify the geometric parameters.

We therefore removed all geometric constraints on the system, re-optimized in $C_1$ symmetry, and found minimum energy geometries at the MP2, B3LYP, and QCISD levels, employing the 6-311++G** basis set; these results were confirmed at the MP2 and B3LYP levels using the aug-cc-pVTZ basis set. From these results, we therefore conclude that the energy minimum on the $O_2^-/H_2S$ potential energy hypersurface is actually a complex between $HS^-$ and $HO_2$, with an out-of-plane geometry, as illustrated in Figure 3. The S atom is almost in the same plane as the hydroperoxy radical, but the hydrogen atom is twisted out of that plane. The optimized parameters are given in Table 2, together with the harmonic vibrational frequencies, where these were calculated. From the form of the vibrations, we can identify them as follows (the descriptions are approximate, since all atoms contribute to each vibration, to an extent). $\omega_1$ is the $HS^-$ stretch; $\omega_2$ is the HO stretch and is $HO_2$-localized; $\omega_3$ is the HOO hydroperoxy bend; $\omega_4$ is the OO stretch; $\omega_5$ is an out-of-plane wag of the OH bond; $\omega_6$ is an in-plane bend resembling an antigearing motion of $HO_2$ and $SH^-$; $\omega_7$ is an in-plane bend that corresponds closely to an internal rotation of the $SH^-$; $\omega_8$ is the intermolecular stretch; and $\omega_9$ is an out-of-plane wag of the $SH^-$.

**Binding Energies.** A determination of the binding energy of the complex was then undertaken. We wished to include the full counterpoise correction in these calculations, but as ever such calculations require some care, particularly in the identi-

fication of the moieties that are to be employed.[17] In the present case, the geometry optimizations and the above discussion indicates that the two moieties that are required are $HS^-$ and $HO_2$.

From Table 2, it will be seen that there are several levels of theory employed to obtain the minimum energy geometry, and it was not obvious which of these to use for the single-point RCCSD(T) calculations. Consequently, we performed RCCSD-(T) single-point calculations at the optimized geometries obtained at the QCISD/6-311++G**, B3LYP/aug-cc-pVTZ, and MP2/aug-cc-pVTZ levels of theory. The lowest energy obtained was at the QCISD/6-311++G** geometry, and so it was this one that was used for the CP-corrected binding energy calculations.

We therefore optimized the geometries of $HO_2$ and $HS^-$ at the QCISD/6-311++G** level of theory. For $HO_2$, the geometry obtained was $R_{OH} = 0.971$ Å, $R_{OO} = 1.335$ Å, and $\theta = 104.7°$; these values compare well with the experimental geometry of $R_{OH} = 0.977$ Å, $R_{OO} = 1.335$ Å, and $\theta = 104.1°$.[18] For $HS^-$, the geometry obtained was $R_{SH} = 1.346$ Å; there does not appear to be an experimental geometry with which to compare this value. We denote these geometries by a superscript "opt" in the equations below. The procedure we used to obtain the counterpoise-corrected binding energies was as follows.

We performed a ghost center calculation on $HO_2$ (where the $SH^-$ basis functions were positioned at the respective positions in the optimized geometry of the complex); we denote this energy by $E(HO_2)^{complex}(SH^-)^G$. We then did the same calculation, but with the ghost functions absent; we denote this energy by $E(HO_2)^{complex}$. We then calculated the basis set superposition error, BSSE from

$$\mathrm{BSSE}(HO_2) = E(HO_2)^{complex} - E(HO_2)^{complex}(SH^-)^G \quad (1)$$

and similarly

$$\mathrm{BSSE}(SH^-) = E(SH^-)^{complex} - E(SH^-)^{complex}(HO_2)^G \quad (2)$$

The uncorrected binding energy was obtained as the difference between the energies of $H_2O$ and $O_2^-$, with the QCISD/6-311++G** geometries being used

$$\Delta E = E(HO_2)^{opt} + E(SH^-)^{opt} - E(HS{-}HO_2) \quad (3)$$

the counterpoise corrected binding energy was then obtained as

$$\Delta E^{CP} = \Delta E + \mathrm{BSSE}(HO_2) + \mathrm{BSSE}(HS^-) \quad (4)$$

We find that $\mathrm{BSSE}(HO_2) = 0.3$ kcal mol$^{-1}$ and $\mathrm{BSSE}(SH^-) = 0.9$ kcal mol$^{-1}$, with $\Delta E = 15.7$ kcal mol$^{-1}$; thus, we obtain $\Delta E^{CP} = 14.4$ kcal mol$^{-1}$; this corresponds to a $D_e$ value.

## V. Discussion

If we compare $O_2^-{-}H_2O$ and "$O_2^-{-}H_2S$", then it is clear from previous calculations[12,13,19] and experiments[19,20] that the former exists in the form indicated. If we consider the reaction

$$O_2^- + H_2O \rightarrow OH^- + HO_2 \quad (5)$$

then using $\Delta H_f^{0K}$ values given in Table 3 allows the reaction enthalpy $\Delta H_r^{0K}$ to be calculated as +37 kcal mol$^{-1}$, consistent with the reaction not taking place; it is unlikely that the binding energy of the $OH{-}HO_2$ complex will be enough to overcome this endothermicity. This is in contrast with the enthalpy of the corresponding reaction with $H_2S$:

$$O_2^- + H_2S \rightarrow SH^- + HO_2 \quad (6)$$

where $\Delta H_r^{0K} = -4$ kcal mol$^{-1}$. [We note, however, that the error in $\Delta H_f^{0K}(HO_2)$ is very large, especially if percentage errors (rather than absolute) are considered, and that at best the latter reaction may be said to be thermoneutral within experimental error.] With the binding energy of the complex of 14.4 kcal mol$^{-1}$ (see above), and even taking into account the error in the calculated $\Delta H_r$, the formation of the complex $HS{-}HO_2$ is expected to be exothermic. (Complex formation will, of course, require a third body for stabilization.) In Table 3, we have derived the $\Delta H_f^{0K}$ value for $HS^-$ by making use of the $\Delta H_f^{0K}$ value for SH from the JANAF tables[18] and adding the electron affinity of SH of 2.317 ± 0.002 eV from ref 21 (a similar, although not identical, value is given in ref 22, derived from a spectrum in ref 21).

**TABLE 3: Heats of Formation for Species Involved in Reactions 1 and 2**

| species | $\Delta H_f$(0 K)/kcal mol$^{-1}$ | source |
|---|---|---|
| $H_2S$ | −4.2 ± 0.2 | JANAF[18] |
| $O_2^-$ | −11.6 ± 0.2 | JANAF[18] |
| $HS^-$ | −20.8 ± 1.2 | [a] |
| $HO_2$ | 1.2 ± 2.0 | JANAF[18] |
| HS | 32.6 ± 1.2 | JANAF[18] |
| $H_2O$ | −57.1[b] | JANAF[18] |
| $OH^-$ | −32.8 ± 0.9 | JANAF[18] |

[a] Derived from $\Delta H_f^{0K}(SH)$[18] and the electron affinity of SH[21], see text. [b] Error <0.1 kcal mol$^{-1}$.

The implication of the collision-induced dissociation evidence is that the complex formed with $m/z = 66$ has the form of $SH^-$ interacting with $HO_2$. One should perhaps query whether this is the structure of the cold complex, or rather that the $SH^-$ produced in the collision-induced dissociation experiments is merely the result of "hot" clusters dissociating. First, the experiments were carried out in an atmospheric source, and therefore the high-collision frequency is expected to lead to a good thermal equilibration of the species (~300 K). At this temperature, although there will be thermal excitation of some of the intermolecular modes in the complex, the excitation of intramolecular modes, that is, ones localized on the constituent monomer moieties, will be essentially zero. Thus, we expect vibrational motion of the intermolecular modes of the complex, but no motion that is likely to lead to the transfer of a proton from $H_2S$ to $O_2^-$, without that transfer being an essential part of the bonding at the minimum energy of the complex. Also, the collision-induced dissociation conditions employed are rather mild, and so again, the observation of $SH^-$ production as a result of these collisions suggests that it is an integral part of the complex and not formed as part of an intracluster reaction. Finally, the ab initio and density functional results, which are performed at the potential energy minimum, with no vibrational excitation, also suggest that the complex between $H_2S$ and $O_2^-$ is actually $HS{-}H_2O$. This is also in line with the thermodynamical considerations, outlined above. We conclude, therefore, that despite our experiments being performed on a thermalized sample, the evidence all points toward the "$H_2S{-}O_2^-$" complex having a proton transferred from $H_2S$ to $O_2^-$. This result is consistent with the results obtained when $I^-$ collides with $H_2S$,[16] where the formation of $HS^-$ was observed when the endothermicity of the reaction was overcome.

For completeness we note that in the IMS studies, the reacting species is unclear; as indicated in Figure 1, the IMS peak is

actually due to $O_2^-$ and its hydrates, and so the reaction with $H_2S$ that produces the "$H_2SO_2^-$" species could either be bare $O_2^-$ or a hydrate thereof. The results of the thermochemical calculations do seem to indicate that the formation of $SH^-$ and $HO_2$ from the reaction of $O_2^-$ with $H_2S$ could be exothermic (but again there is uncertainty on the calculated exothermicity). The presence of an activation energy barrier is possible, which would be overcome by kinetic energy of the $O_2^-$. The geometry optimizations appear to indicate that there is no barrier for the reaction, since optimizations that commenced with a clear $H_2S$ moiety interacting with $O_2^-$ efficiently optimized into $HS-HO_2$. We conclude, therefore, that $O_2^-$ reacts with $H_2S$ to form $HS-HO_2$. The mass spectrometry results of the collision-induced dissociation experiments, shown in Figure 2, are particularly clear on this point: the complex clearly is broken up in the electric field region around the orifice, with $HS^-$ being one of the fragments.

## VI. Conclusions

The results from ion mobility spectrometry, mass spectrometry, thermodynamics, and ab initio and DFT calculations all point to the fact that the "$H_2SO_2^-$" species observed in the IMS and mass spectrometric studies is a complex of the form $HS-HO_2$. In the case where a bare $O_2^-$ reacts with $H_2S$, the reaction is essentially a proton transfer from $H_2S$ to the $O_2^-$. The indications also are that there is a negligible barrier to proton transfer. We calculate a value of $D_e = 14.4$ kcal mol$^{-1}$ for the binding energy of $HS-HO_2$. Of course, this study does not take into account any solvent effects that would be present in solution, but consideration needs to be given to the implication of the present results that $H_2S$ reacts with $O_2^-$ to produce $HS-O_2$, which may then undergo further reaction.

Clearly, it would be of interest to interrogate the "$H_2S-O_2^-$" complex spectroscopically, either in the gas phase or in inert matrixes, since infrared spectroscopy should provide unequivocal evidence regarding the bonding in this species; negative ion photoelectron spectroscopy is also a possibility for study.

**Acknowledgment.** T.G.W. is grateful to the EPSRC for the award of computer time at the Rutherford Appleton Laboratories under the auspices of the Computational Chemistry Working Party (CCWP), which enabled these calculations to be performed.

## References and Notes

(1) Kimura, H. *Biochem. Biophys. Res. Commun.* **200**, *267*, 129.
(2) Abe, K.; Kimura, H. *J. Neurosci.* **1996**, *6*, 1066.
(3) Eto, K.; Asada, T.; Arima, K.; Makifuchi, T.; Kimura, H. *Biochem. Biophys. Res. Commun.* **2002**, *293*, 1485.
(4) Kamoun, P.; Belardinelli, M. C.; Chabli, A.; Lallouchi, K. *Am. J. Med. Genet. A* **2003**, *116*, 310.
(5) Geng, B.; Chang, Lin; Pan, C.; Qi, Y.; Zhao, J.; Pang, Y.; Du, J.; Tang, C. *Biochem. Biophys. Res. Commun.* **2004**, *318*, 756.
(6) Kolehmainen, M.; Ruuskanen, J.; Rissanen, E.; Raatikainen, O. *J. Air Waste Manage. Assoc.* **2001**, *51*, 966.
(7) Steiner, W. E.; Clowers, B. H.; Haigh, P. E.; Hill, H. H. *Anal. Chem.* **2003**, *75*, 6068.
(8) Ewing, R. G.; Atkinson, D. A.; Eiceman, G. A.; Ewing, G. J. *Talanta* **2001**, *54*, 515.
(9) Kambara, H.; Mitsui, Y.; Kanomata, I. *Anal. Chem.* **1979**, *51*, 1447.
(10) Ross, S. K.; Bell, A. J. *Int. J. Mass Spectrom.* **2002**, *218*, L1.
(11) Skalny, J. D.; Mikoviny, T.; Matejcik, S.; Mason, N. J. *Int. J. Mass Spectrom.* **2004**, *233*, 317.
(12) Robinson, E. M. C.; Holstein, W. L.; Stewart, G. M.; Buntine, M. A. *Phys. Chem. Chem. Phys.* **1999**, *1*, 3961.
(13) Bell, A. J.; Wright, T. G. *Phys. Chem. Chem. Phys.* **2004**, *6*, 4385.
(14) Gaussian 03, Frisch, M. J. et al. Gaussian Inc.: Pittburgh, PA, 2003.
(15) MOLPRO is a package of ab initio programs written by Werner, H.-J.; Knowles, P. J. et al.
(16) Refaey, K. M. A. *J. Chem. Phys.* **1976**, *65*, 2002.
(17) van Duijneveldt, F. B.; van Duijneveldt-van de Rijdt, J. G. C. M.; van Lenthe, J. H. *Chem. Rev.* **1994**, *94*, 1873.
(18) Chase, M. W., Jr. *NIST-JANAF Themochemical Tables*, 4th ed.; J. Phys. Chem. Ref. Data, Monograph 9, 1998.
(19) Weber, J. M.; Kelley, J. A.; Robertson, W. H.; Johnson, M. A. *J. Chem. Phys.* **2001**, *114*, 2698.
(20) Luong, A. K.; Clements, T. G.; Resat, M. S.; Continetti, R. E. *J. Chem. Phys.* **2001**, *114*, 3449.
(21) Kitsopoulos, T. N.; Waller, I. M.; Loeser, J. G.; Neumark, D. M. *Chem. Phys. Lett.* **1989**, *159*, 300.
(22) Shiell, R. C.; Hu, X. K.; Hu, Q. J.; Hepburn, J. W. *J. Phys. Chem. A* **2000**, *104*, 4339.